Elucidating the Spatial Arrangement of Emitter Molecules in Organic Light-Emitting Diode Films

Claire Tonnelé[+], Martin Stroet[+], Bertrand Caron, Andrew J. Clulow, Ravi C. R. Nagiri, Alpeshkumar K. Malde, Paul L. Burn,* Ian R. Gentle, Alan E. Mark,* and Benjamin J. Powell

Abstract: *The effect of varying the emitter concentration on the structural properties of an archetypal phosphorescent blend consisting of 4,4′-bis(N-carbazolyl)biphenyl and tris(2-phenylpyridyl)iridium(III) has been investigated using non-equilibrium molecular dynamics (MD) simulations that mimic the process of vacuum deposition. By comparison with reflectometry measurements, we show that the simulations provide an accurate model of the average density of such films. The emitter molecules were found not to be evenly distributed throughout film, but rather they can form networks that provide charge and/or energy migration pathways, even at emitter concentrations as low as ≈ 5 weight percent. At slightly higher concentrations, percolated networks form that span the entire system. While such networks would give improved charge transport, they could also lead to more non-radiative pathways for the emissive state and a resultant loss of efficiency.*

Small molecule light-emitting layers in organic light-emitting diodes (OLEDs) typically have the emissive molecule blended at low concentration in a host matrix to avoid luminescence quenching intermolecular interactions.[1] It is generally assumed that at the low concentrations [1–10 weight percent (wt %)] used, the emissive guests are evenly distributed throughout the host. Indeed, neutron reflectometry (NR) measurements show that the archetypical phosphorescent emissive layer, 6–12 wt % of *fac*-tris(2-phenylpyridyl)iridium(III) [Ir(ppy)$_3$] in 4,4′-bis(*N*-carbazolyl)biphenyl (CBP), has an even concentration of Ir(ppy)$_3$

throughout the depth of the film.[2] However, currently available experimental methods lack the resolution required to locate each Ir(ppy)$_3$ guest molecule within the film, and thus there is little direct experimental evidence that the guest molecules are isolated or evenly distributed. NR measurements, for example, cannot distinguish between whether the Ir(ppy)$_3$ are isolated or form dimers or even larger clusters in the film. The spatial distribution of the guest and host molecules in a film is important for understanding the behavior of phosphorescent emitters used in OLEDs, as well as other materials such as thermally-activated delayed fluorescence emitters[3,4] and low donor content solar cells.[5]

Films of phosphorescent light-emitting materials can undergo triplet–triplet annihilation (TTA), with the level dependent on the spatial distribution of the emitters.[6] Förster-type TTA tends to be inefficient for low concentration blends of emissive iridium(III) complexes due to poor spectral overlap of their emission and absorption spectra. In contrast, if the emitters are in close proximity, triplet excitons on adjacent molecules can annihilate through Dexter-type interactions, with the rate being exponentially dependent on the distance between the donor and acceptor.[1] Thus, Dexter-based TTA will increase with doping concentration as the average distance between emitters decreases.[7–10] The arrangement of the guest and host molecules in a film is dependent on the deposition process and any post-deposition annealing.

Computational methods provide a way to gain insight into the effect of the spatial distribution of emitters within a host matrix on the properties of devices.[11] Ratcliff et al.[12] have mimicked the process of deposition of an 8 wt % Ir-(ppy)$_3$:CBP blend using a Monte Carlo procedure in which individual molecules with a fixed geometry were added sequentially in a fixed order to a growing layer. The coordinates of each molecule added were then frozen, which ensured the emitter molecules were uniformly distributed within the matrix. Herein, we report non-equilibrium molecular dynamics (MD) simulations of the vacuum deposition of an Ir(ppy)$_3$:CBP layer (Figure 1). The parameters used to describe both CBP and Ir(ppy)$_3$ were optimized

[*] C. Tonnelé,[+] A. J. Clulow, R. C. R. Nagiri, P. L. Burn, I. R. Gentle
Centre for Organic Photonics & Electronics
School of Chemistry and Molecular Biosciences
The University of Queensland
St Lucia Campus, Brisbane 4072 (Australia)
E-mail: p.burn2@uq.edu.au

M. Stroet,[+] B. Caron, A. K. Malde, A. E. Mark
Molecular Dynamics Group
School of Chemistry and Molecular Biosciences
The University of Queensland
St Lucia Campus, Brisbane 4072 (Australia)
E-mail: a.e.mark@uq.edu.au

B. J. Powell
Centre for Organic Photonics & Electronics
School of Mathematics and Physics
The University of Queensland
St Lucia Campus, Brisbane 4072 (Australia)

[+] These authors contributed equally to this work.

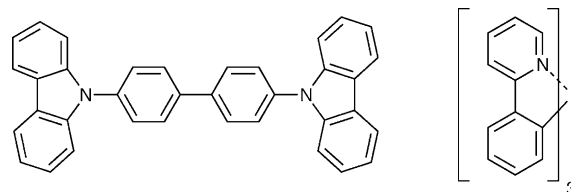Supporting information for this article can be found under:
http://dx.doi.org/10.1002/anie.201610727.

Figure 1. Chemical structures of CBP (left) and Ir(ppy)$_3$ (right).

against experimental data and quantum mechanical calculations (Supporting Information). We find that even at 2 wt% of Ir(ppy)$_3$ in CBP, not all of the emitter molecules can be considered as isolated, and at concentrations as low as 14 wt% the Ir(ppy)$_3$ molecules are highly interconnected with percolated pathways extending throughout the film.

Non-equilibrium atomistic simulations of the vacuum deposition of Ir(ppy)$_3$ and CBP onto a single layer of graphene were performed (Supporting Information). Graphene provides a flat uniform non-polar surface to which CBP weakly binds so as to minimize the induction of structure and ensure rapid relaxation of the CBP matrix in the simulations. For the main study, the emission layers were generated by randomly releasing individual molecules of either CBP, Λ-*fac*-Ir(ppy)$_3$, or Δ-*fac*-Ir(ppy)$_3$ above the surface, and allowing them to bind spontaneously to the layer with target blend

ratios of 0, 2, 6, 15, or 30 wt% of the Ir(ppy)$_3$. The actual numbers of CBP and Ir(ppy)$_3$ molecules in each simulated blend were similar to that expected (Table S3). In addition, the single Λ-*fac*-Ir(ppy)$_3$ isomer was also deposited at a nominal 6 wt% to determine whether enantiopure and racemic mixtures of emitters give rise to a similar guest distribution. The process of deposition was highly dynamic, with the CBP molecules in particular sampling a range of conformational states both in the gas phase and once bound to the surface. Molecules within the uppermost layers also continued to diffuse across the surface after initial binding. This suggests that freezing the positions of molecules once embedded within the growing layer, as proposed by Ratcliff et al.,[12] restricts equilibration within the system and leads to an inappropriate film morphology. Figure 2 shows side views of snapshots of the final vacuum-deposited racemic Ir(ppy)$_3$
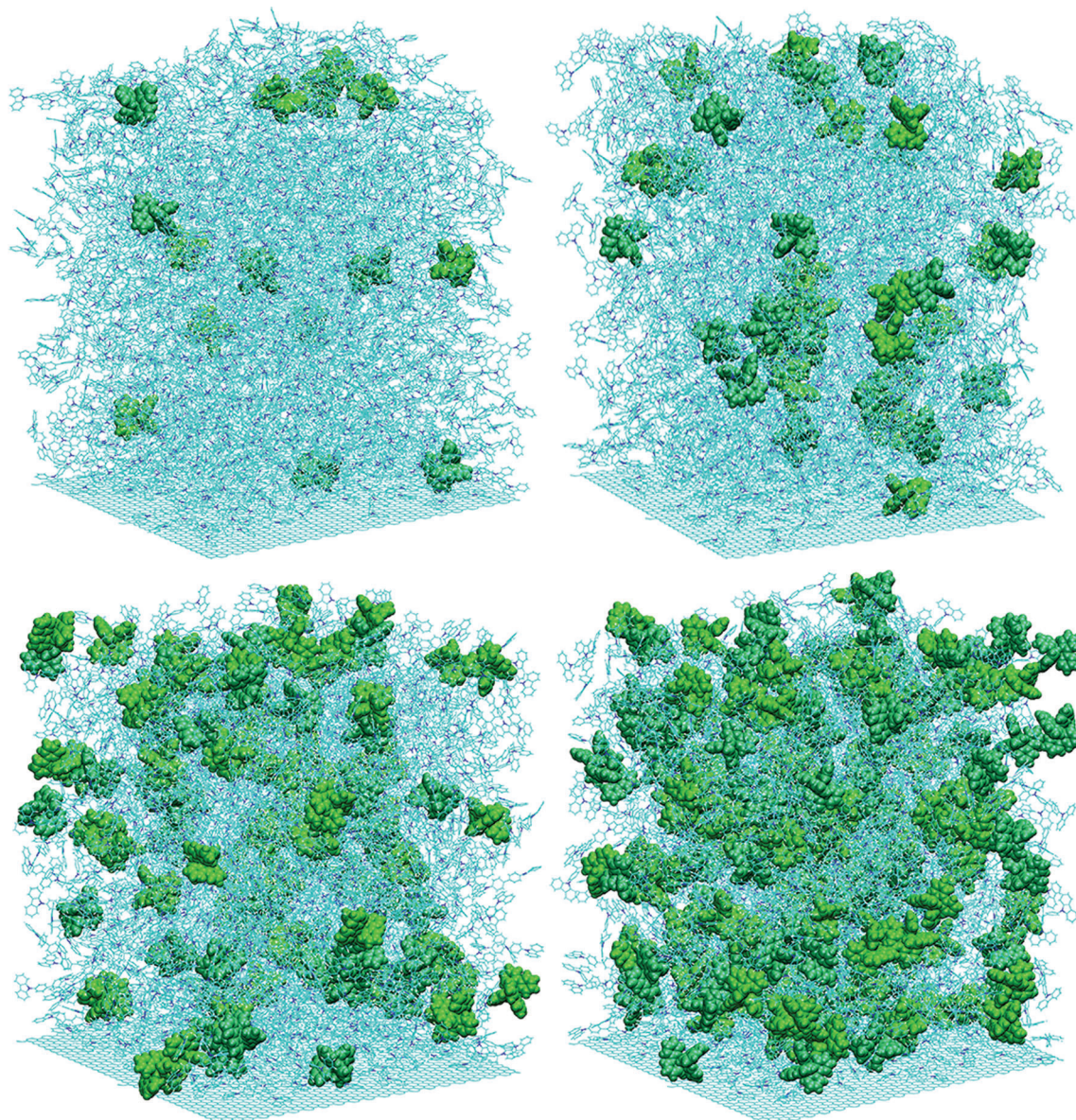
Figure 2. Snapshots of the final vacuum-deposited blends (last frame of equilibration) of 2.0, 5.3, 14.1, and 26.3 wt% (reading from top and left to right) viewed perpendicular to the graphene substrate (along the *y*-axis). The Ir(ppy)$_3$ molecules (green) are shown in a space-filling representation. The CBP molecules are shown in a line representation. The graphene substrate lies in the *x*−*y* plane and sits just below the bottom of each Figure. The different shades of green distinguish the two Ir(ppy)$_3$ enantiomers.

containing blends (last frame of equilibration) of 2.0, 5.3, 14.1, and 26.3 wt %. It is clear that the racemic Ir(ppy)$_3$ emitter molecules are neither evenly distributed as single molecules throughout the film nor form distinct clusters.

An important although challenging test of the accuracy of the deposition simulations (the time scale of the simulations deposition is short compared to typical experiments) is the ability to reproduce experimental density profiles normal to the plane of the layer. X-ray and neutron reflectivity profiles for a 6.4 wt % racemic Ir(ppy)$_3$-containing blend are shown in Figure S4. The average mass density for the 6.4 wt % racemic Ir(ppy)$_3$-containing blend derived from the optimized neutron and X-ray scattering length densities of 2.55 and 11.3 × 10^{-4} nm^{-2}, respectively, was 1.27 g cm^{-3}. The mass density profiles perpendicular to the graphene layer for each of the racemic Ir(ppy)$_3$-containing blends simulated in this work are shown in Figure S5. The total density is shown as well as the individual densities for the CBP and racemic Ir(ppy)$_3$ molecules. Apart from a sharp initial peak in the density profile in each of the simulated systems corresponding to CPB molecules in the first layer lying flat against the graphene, the density profiles show no evidence of long-range order, in line with that observed experimentally. The high density layer at the substrate interface was not resolvable in the X-ray and neutron reflectivity modeling as it was thinner than the thinnest observable features defined by πQ_{max}^{-1}, where Q_{max} is the Q value at which the background intensity of the measurement was reached. The average densities of the different racemic Ir(ppy)$_3$-containing blends obtained in the simulations are listed in Table S3, and range from 1.16 g cm^{-3} in the case of the pure CBP film up to 1.23 g cm^{-3} for the 26.3 wt % racemic Ir(ppy)$_3$-containing blend. Overall, the calculated densities for the different blends compare well to the experimental value of 1.27 g cm^{-3} for the 6.4 wt % racemic Ir(ppy)$_3$ blend. The slight underestimation of the density in the simulations is most likely due to the layer thickness −10 nm versus 40 nm in the experiment, and short annealing time; the 10–20 ns simulated annealing is much less than what would occur under normal deposition conditions, and therefore the films may still not be optimally packed. The 2.0 wt % simulation was not annealed and it is evident that the uppermost part of the layer extends further into the vacuum layer and is less dense than in the other systems. Finally, while the simulations show the total density is uniform across the layer, there appears to be a very slight accumulation of the Ir(ppy)$_3$ molecules adjacent to the vacuum layer in each of the blends. However, this ≤ 1 nm thick accumulation layer cannot be confirmed by NR experiments, as it is again less than the resolvable feature width, even when selective deuteration is used to give additional contrast.[13]

Figure 3 shows the excess orientation order with respect to the graphene layer, where 1.0 represents a fully ordered sample and 0.0 a random distribution of angles for a pure CBP layer and for the 5.3 wt % racemic Ir(ppy)$_3$-containing blend. In line with the density profiles (Figure S5), the first layer of CBP molecules in contact with the graphene layer are highly ordered, as are molecules in contact with the vacuum. However, this order only extends 1–2 nm into the material beyond which the CBP molecules show no preferred ori-
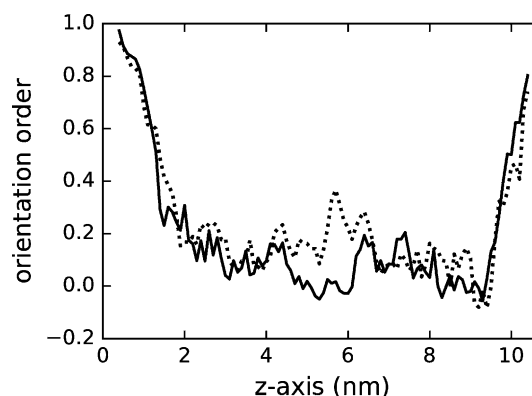

Figure 3. The excess orientational order of the CBP molecules as a function of the distance from the graphene substrate, where 1.0 represents a system in which all of the CBP molecules lie in the plane of the graphene substrate, 0 a uniform distribution of orientations, and −1.0 a system in which all of the molecules lie perpendicular to the plane of the graphene substrate. Pure CBP (solid line) and 5.3 wt % Ir(ppy)$_3$ (dotted line).

entation, which is consistent with ellipsometry measurements (Supporting Information). Inclusion of racemic Ir(ppy)$_3$ in the film has no obvious effect on the degree of order of the CBP, and the Ir(ppy)$_3$ molecules also show no preferred orientation with respect to the graphene. Figure 4 shows the distribution of the angles between the Ir(ppy)$_3$ C$_3$ symmetry axes and the normal to the plane of the graphene substrate (z-axis) compared with that expected for a random distribution. Note, the curve in Figure 4 was obtained by combining results from all of the racemic Ir(ppy)$_3$-containing blends to improve statistics. Results obtained for the 6 wt % Λ-*fac*-Ir(ppy)$_3$:CBP blend were similar to the 5.3 wt % racemic Ir(ppy)$_3$-containing blend. Thus, the simulations lead to a film morphology in which neither the Ir(ppy)$_3$ (racemic or enantiomerically pure) nor the CBP molecules adopt a preferred orientation in the bulk with respect to the substrate layer, which is consistent with experimental results.[14]
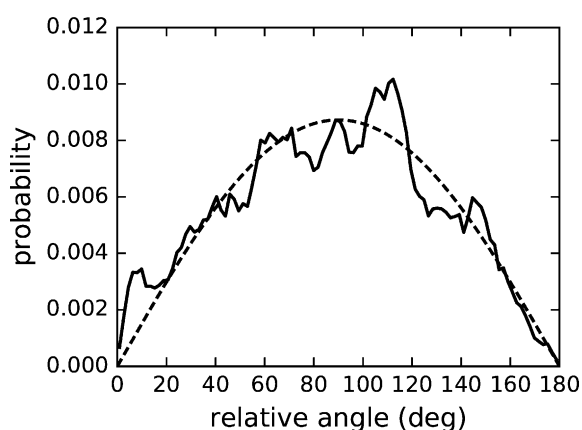

Figure 4. Distribution of the angle between the Ir(ppy)$_3$ C$_3$ symmetry axis and the normal to the plane of the graphene substrate (z-axis). The solid line corresponds to the combination of data from all of the racemic Ir(ppy)$_3$-containing blends studied [2.0, 5.3, 14.1, and 26.3 wt % Ir(ppy)$_3$]. The dashed line shows the expected curve for a random distribution of orientations.

From Figure 2, it is evident that the racemic emitter molecules are not uniformly distributed in the film. To determine whether the emitter molecules are randomly distributed or if there is a preferential interaction between the Ir(ppy)$_3$ complexes, the radial distribution function (RDF) of the center of mass of the Ir(ppy)$_3$ molecules (effectively the position of the iridium atom) was calculated for each blend containing racemic Ir(ppy)$_3$ (Figure S7). The statistics at 2.0 wt% were insufficient to draw any conclusions, but at 5.3, 14.1, and 26.3 wt% there is a clear peak at approximately 1 nm that is considerably larger than that expected for hard spheres at an equivalent packing density. This indicates that the racemic Ir(ppy)$_3$ molecules preferentially associate and are not randomly distributed within the blend, with the interactions most pronounced in the 5.3 wt% blend (similar to the concentration that gives the best OLED performance), and that the distribution becomes more uniform for the higher wt% films. The 6 wt% Λ-*fac*-Ir-(ppy)$_3$:CBP blend also shows a peak at approximately 1 nm, indicating that even pure enantiomers can pack closely in a blend. However, care must be taken not to over-interpret the results as they are based on relatively small systems and subject to statistical uncertainty.

As the RDFs show that the racemic and enantiopure Ir(ppy)$_3$ emitters co-locate in the film, the extent to which the emitters formed interconnected networks in the different blends was studied. The connectivity between the racemic Ir(ppy)$_3$ molecules in the film was analyzed using the distances between the centers-of-mass of the Ir(ppy)$_3$ molecules of the final configuration of each simulated system. The extent of connectivity was calculated for a series of cut-off distances (1.25, 1.50, 1.75, and 2.00 nm). Given that the effective diameter of an Ir(ppy)$_3$ molecule is ≈1.0 nm (Figure S7), these distances correspond to a separation of the racemic emitters of less than 0.25, 0.50, 0.75, and 1.00 nm, respectively. The results expressed in terms of the average number of connected neighbors, the percentage of racemic emitters without any neighbors, the maximum connected distance, as well as the maximum lateral and vertical connected distances for each blend and each cut-off are given in Table S4. It was found there is a dramatic increase in the connectedness within the system upon going from 2.0 wt% to 14.1 wt%. At 2 wt%, the majority of the racemic emitters are isolated. Even using a cut-off of 2.00 nm, the average number of neighbors is only 0.1, although both Figures 2 and 5 show that for the racemic-containing blend some Ir(ppy)$_3$ molecules lie in close proximity. At 5.3 wt%, ≈50% of the emitters in the racemic blend have another emitter within 0.25 nm, with ≈90% having another emitter within 1.00 nm leading to networks of emitters that extend over a distance of >8 nm. Increasing the concentration of Ir(ppy)$_3$ in the racemic blend drives a percolation transition. At 14.1 wt%, networks extend across half the box even using the shortest cut-off, with a 1.75 nm cut-off showing networks extending throughout the entire blend. The effect of increasing the Ir(ppy)$_3$ concentration in the racemic blend on the extent of network formation is illustrated in Figure 5 (other cut-off distances are shown in Figure S8), which shows the extent of network formation for the different blends exam-
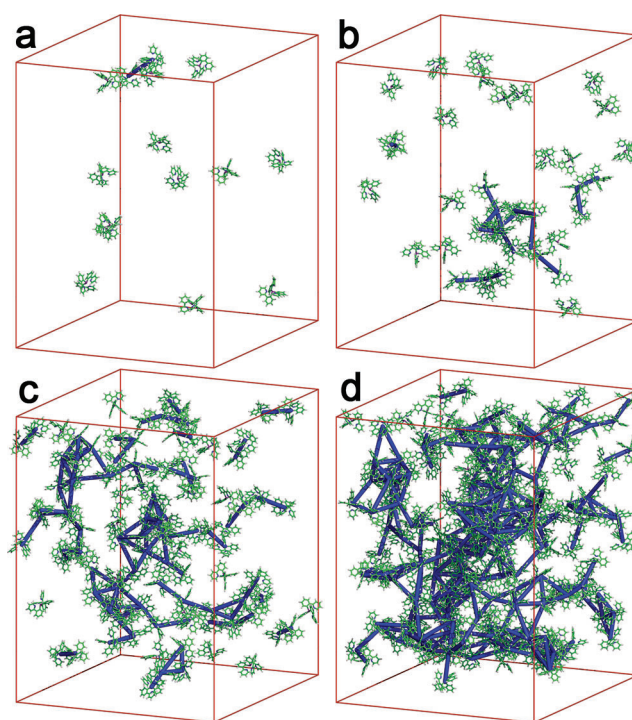
Figure 5. Ir(ppy)$_3$ connectivity network for a center-of-mass neighbor cut-off distance of 1.5 nm (shown with blue lines) for a) 2.0 wt%, b) 5.3 wt%, c) 14.1 wt%, and d) 26.3 wt%. Connections through a periodic boundary have been omitted for clarity.

ined using a cut-off of 1.5 nm between the centers-of-mass of the Ir(ppy)$_3$ molecules. As can be seen even using this cut-off distance, extended network formation is evident at 14.1 wt%, while at 26.3 wt% the emitter molecules in the racemic blend are almost fully interconnected. A similar level of connectivity was seen for the blend containing the enantiopure Ir(ppy)$_3$ molecules (Figure S9 and Table S5).

The results of the simulations have important implications for OLEDs. They suggest that at typical dopant concentrations some, if not all, emitters are likely to be in sufficiently close proximity to other emitters to affect not only the luminescence of the emitters but also charge mobility. In the case of Ir(ppy)$_3$:CBP blends, the ionization potential and electron affinity of the Ir(ppy)$_3$ sit within those of the CBP, and thus an isolated Ir(ppy)$_3$ molecule should act as a charge trap. However, the simulations suggest that films with an Ir(ppy)$_3$ concentration ≥5.3 wt% will contain networks of molecules through which charges could migrate and sample more of the film, with the largest change occurring at the percolation transition. In such a case, it would be expected that the overall mobility of the film would be higher than the situation when the Ir(ppy)$_3$ was evenly dispersed in the CBP. Furthermore, the connectivity of the Ir(ppy)$_3$ emitters might be expected to increase TTA. Isotropic emitting Ir(ppy)$_3$:CBP OLEDs can have an external quantum efficiency of 18%,[14] which suggests that a degree of emitter interaction might not be very detrimental to the emission at low current/excitation densities. However, the roll off (and its rate) in performance seen at higher densities will be strongly dependent on the degree of interconnectivity between the Ir(ppy)$_3$ dopants.

4   www.angewandte.org

↞↞ These are not the final page numbers!

© 2017 Wiley-VCH Verlag GmbH & Co. KGaA, Weinheim

Angew. Chem. Int. Ed. **2017**, *56*, 1–6

That the optoelectronic properties of organic semiconductor materials are influenced by the surrounding environment and energetic landscape in these films is well recognized. The results of the simulations suggest that the properties of the blends considered in this work are more complex than generally assumed as the emissive Ir(ppy)$_3$ can sit in a range of local environments, with varying numbers of nearby Ir(ppy)$_3$ and CBP. Thus it is important to obtain the spatial arrangement of emitters within a blend before performing electronic structure calculations of the optoelectronic properties.

An atomistic molecular dynamics procedure has been used to mimic co-evaporation of Ir(ppy)$_3$:CBP films. The study focused on racemic Ir(ppy)$_3$:CBP blends as these are used in typical OLEDs, although the enantiopure Ir(ppy)$_3$-containing film of similar wt% showed similar characteristics. It was found that only at the lowest ratio (2.0 wt%) the racemic Ir(ppy)$_3$ could be considered as isolated. At the dopant concentrations typically used in OLEDs, a significant number of Ir(ppy)$_3$ molecules were found to be in close proximity to other emitters. At concentrations approaching 14 wt%, the Ir(ppy)$_3$ molecules formed percolated networks that spanned the entire film. Given the relevant energy levels of the Ir(ppy)$_3$ and CBP, this could lead to more efficient charge transport throughout the films. However, the connectivity of the Ir(ppy)$_3$ within the films would also be expected to give rise to increased TTA, particularly at high current densities. This would lead to the roll off in efficiency that is normally observed in phosphorescent OLEDs. These results help to explain the behavior of OLEDs but also have important ramifications for all semiconductor devices comprising blends in which one of the components is at a low concentration.

Acknowledgements

Conflict of interest

The authors declare no conflict of interest.

[1] D. L. Dexter, J. H. Schulman, *J. Chem. Phys.* **1954**, *22*, 1063–1070.

[2] A. R. G. Smith, J. L. Ruggles, H. Cavaye, P. E. Shaw, T. A. Darwish, M. James, et al., *Adv. Funct. Mater.* **2011**, *21*, 2225–2231.

[3] D. Volz, *J. Photonics Energy* **2016**, *6*, 020901.

[4] Y. Tao, K. Yuan, T. Chen, P. Xu, H. H. Li, R. F. Chen, et al., *Adv. Mater.* **2014**, *26*, 7931–7958.

[5] D. M. Stoltzfus, J. E. Donaghey, A. Armin, P. E. Shaw, P. L. Burn, P. Meredith, *Chem. Rev.* **2016**, *116*, 12920–12955.

[6] M. A. Baldo, C. Adachi, S. R. Forrest, *Phys. Rev. B* **2000**, *62*, 10967–10977.

[7] W. Staroske, M. Pfeiffer, K. Leo, M. Hoffmann, *Phys. Rev. Lett.* **2007**, *98*, 197402.

[8] S. Reineke, G. Schwartz, K. Walzer, M. Falke, K. Leo, *Appl. Phys. Lett.* **2009**, *94*, 163305.

[9] E. B. Namdas, A. Ruseckas, I. D. W. Samuel, S. C. Lo, P. L. Burn, *Appl. Phys. Lett.* **2005**, *86*, 091104.

[10] J. C. Ribierre, A. Ruseckas, K. Knights, S. V. Staton, N. Cumpstey, P. L. Burn, et al., *Phys. Rev. Lett.* **2008**, *100*, 017402.

[11] P. Kordt, J. J. M. van Holst, M. Al Helwi, W. Kowalsky, F. May, A. Badinski, C. Lennartz, A. Andrienko, *Adv. Funct. Mater.* **2015**, *25*, 1955.

[12] L. E. Ratcliff, L. Grisanti, L. Genovese, T. Deutsch, T. Neumann, D. Danilov, et al., *J. Chem. Theory Comput.* **2015**, *11*, 2077–2086.

[13] T. A. Darwish, A. R. G. Smith, I. R. Gentle, P. L. Burn, E. Luks, G. Moraes, et al., *Tetrahedron Lett.* **2012**, *53*, 931–935.

[14] P. Liehm, C. Murawski, M. Furno, B. Lussem, K. Leo, M. C. Gather, *Appl. Phys. Lett.* **2012**, *101*, 253304.
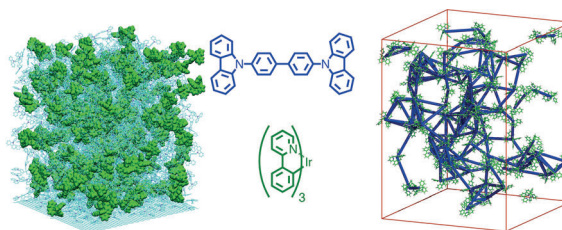
Communications

Light-Emitting Diodes

C. Tonnelé, M. Stroet, B. Caron,
A. J. Clulow, R. C. R. Nagiri, A. K. Malde,
P. L. Burn,* I. R. Gentle, A. E. Mark,*
B. J. Powell ————— ▮▮▮▮–▮▮▮▮

Elucidating the Spatial Arrangement of
Emitter Molecules in Organic Light-
Emitting Diode Films

The distribution of triplet emitters in molecular hosts for organic light-emitting diodes was investigated using a combination of simulations and experimenta-tion. At relatively low guest concentrations, triplet emitters were found to cluster, forming possible percolation pathways for charge carriers.